Tellus (2000), 52A, 190–202
Printed in UK. All rights reserved

TELLUS
ISSN 0280–6495

Explanations for simultaneous laminae in water vapor and aerosol profiles found during the SESAME experiment

By H. TEITELBAUM*, C. BASDEVANT and M. MOUSTAOUI, *Laboratoire de Météorologie Dynamique, École Normale Supérieure, 24 rue Lhomond, 75231 Paris Cedex 05, France*

(Manuscript received 22 March 1999; in final form 11 October 1999)

ABSTRACT

An instrumented balloon launched from Kiruna during the SESAME experiment displayed simultaneous local decreases of water vapor and aerosol at 2 different potential temperature levels 410 K and 364 K. Despite the similar characteristics present at both levels, 2 different explanations are given for these laminae. At the highest level, the air mass showing the water vapor and aerosol decrease is found when the balloon travels in the vortex edge region. A back trajectory shows that this air mass was trapped in the vortex edge region for several days and processed by a PSC causing the water vapor and aerosol decreases. On the other hand, the lowest level air mass was found to be in the sub-vortex region. No local conditions can explain the observed decreases of water vapor and aerosol. Back trajectories show that this air mass originates from middle latitudes. Although the back trajectories calculated in these conditions are more subject to caution, comparison of several characteristics at the measurement point and at the middle latitude sites corroborates the explanation of the decrease of water vapor and aerosol by the origin of the air mass.

1. Introduction

In this paper, we try to explain some characteristics of stratospheric water vapor and aerosol profiles measured simultaneously during the Second European Stratospheric and Mid-Latitude Experiment (SESAME).

Both aerosol and water vapor profiles show simultaneous localized decreases around 410 K and 364 K potential temperature levels. This type of localized decrease has often been observed in ozone profiles. They have been named "laminae" by Dobson (1973), who was the first to point out the existence of such laminated structures of ozone during ozonesonde ascents. Later on, several authors quoted such irregularities in ozone and other minor atmospheric constituents and gave tentative explanations for their existence. Reid and Vaughan (1991, 1993) attributed the ozone laminae to the fact that the measured column was formed with air layers coming from different places with different ozone contents. Newman et al. (1996) explained the ozone laminae they observed by the Rossby wave breaking during the breakdown of the polar vortex. After Mariotti et al. (1977), the transport of air out of the vortex by filaments causes also ozone laminae, although transport by different types of waves can also produce such kind of irregularities (Holton, 1987; Teitelbaum et al., 1996). Numerical modeling (Orsolini et al., 1997) and trajectory calculations (Manney et al., 1998) have also been used to explain the ozone laminae. Layers of very low ozone concentration were observed by Vaughan and Timmis (1998), over Europe; they used calculated back trajectories together with potential vorticity values to conclude that the air masses

* Corresponding author.
e-mail: teitel@lmd.ens.fr

with low ozone content were coming from the sub-tropical troposphere.

Simultaneous laminae in 2 or more minor atmospheric constituents have also been found. Kley et al. (1980) show a simultaneous increase of water vapor and decrease of ozone at the same altitude. After Brasseur and Solomon (1998), this structure suggests that the air must have been advected in a time shorter than small-scale diffusion. Orsolini et al. (1998) studied layered structures in nitrous oxide, methane and halocarbons together with ozone and water vapor. In the case of quasi-simultaneous measures of ozone and water vapor, and contrary to what was found by Kley et al. (1980), both profiles show a decrease at the 400 K level. A numerical modelisation, using a high resolution model, provided a quantitative agreement with the measurements. Jost et al. (1998) showed laminated structures in nitrous oxide, and ozone in the tropical stratosphere they explained by the transport of mid-latitude air into the tropics.

In this paper, we study for the first time the causes of simultaneous laminae in water vapor and aerosol. Furthermore, the same phenomenon appears at 2 different stratospheric levels during the same balloon flight. Despite the apparent similarity of the phenomena at both levels, we shall show that their causes are very different, and they will be analyzed separately.

The highest altitude (410 K) decrease is found to occur in an air parcel located just inside the vortex edge region. A backward trajectory shows that this air parcel has been trapped inside this region at least 7 days before, and that it has presumably been processed by a polar stratospheric cloud (PSC). The fact that the air parcel was trapped inside the vortex edge region is a consequence of the quasi-impermeability of this region. This is a robust feature for the trajectory calculation and it has been used in Teitelbaum et al. (1998) to explain local ozone column measurements. To increase confidence in the attributed origin of the air parcel, we used the method of Vaughan and Timmis (1998), comparing the values of the Ertel potential vorticity (EPV) at both ends of the trajectory.

The lowest-level decrease (364 K) is located in the sub-vortex region and the backward trajectories show that it comes from a latitude where water vapor and aerosol have lowest values than in the vicinity of the measurement point. The EPV test was also used in this case.

In Section 2 we describe the data and give a succinct explanation of the technique and conditions of the experiment. Section 3 deals with a general approach of the concept of vortex edge region, a concept we use to follow the 410 K air mass backward in time, up to the point where it has been processed by the PSC. In Section 4 we present the evidence that suggests the 364 K air mass comes from lower latitudes. Finally, some comments and conclusions are given in Section 5.

2. The measurement technique and the data

During the SESAME experiment, 3 balloon flights instrumented for water vapor and aerosol profile measurements were launched from Kiruna in Sweden (67.9°N, 21.1°E). The payload comprised a frost-point hygrometer, an aerosol counter together with pressure and temperature sensors. The frost-point hygrometer was a classical one (Mastenbrook, 1968; Ovarlez et al., 1987). The aerosol counter was a laser diode particle counter similar to those used for clean room monitoring. It is based on the measurement of the intensity of forward-scattered light by the particles as they pass through a laser-illuminated sensing volume.

Fig. 1 displays the water vapor and aerosol profiles measured during the flight performed on 13 February 1995. The highest level water vapor laminae shows a decrease of around 0.5 ppmv, whereas the lowest reaches 1 ppmv. The aerosol profiles have been measured during the ascending and descending parts of the balloon flight, showing laminae at the same levels as in the water vapor profile. The similarity between both aerosol profiles indicates the good performance of the measuring instrument. The water vapor profile has been measured during the descending part when the balloon was at 68°N, 28°E. The measured temperature profiles, shown in Fig. 2, are characteristic of this region in winter. We note the agreement between the temperature profiles measured in the ascending and the descending part of the flight. In Fig. 2 are also plotted the temperature profiles, obtained from the European Center for Medium-range Weather Forecasts (ECMWF) analysis. They show, between 420 K and 500 K,

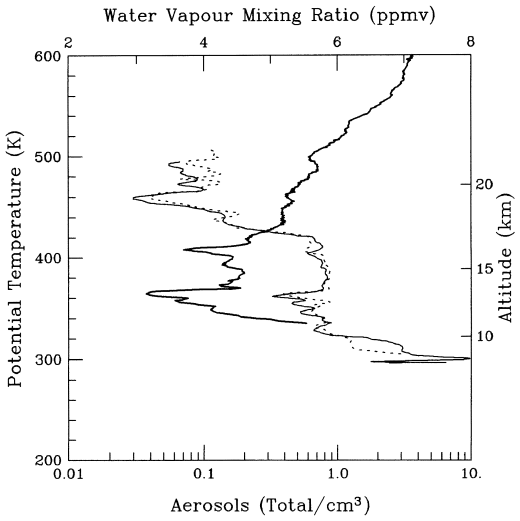

Fig. 1. Vertical profiles measured on 13 February 1995 by an instrumented balloon launched from Kiruna (67.9°N, 21.1°E). Water vapor mixing ratio (thick full line), aerosol during ascending part of the flight (thin full line) and aerosol during descending part of the flight (dotted line). The water vapor profile has been measured during the descending part when the balloon was at 68°N, 28°E.

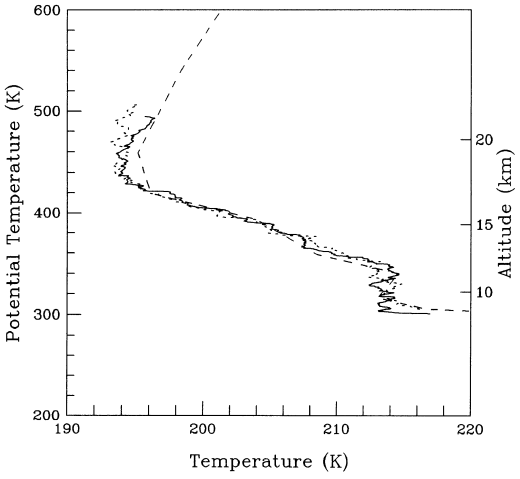

Fig. 2. Temperature profile measured during the same flight as that for Fig. 1. Ascending flight (full line), descending flight (dotted line). The temperature profile obtained from ECMWF analysis is also shown (dashed line).

temperatures higher than that measured. This bias is in agreement with the results obtained by Knudsen et al. (1996), showing that such difference occurs often at local temperature minima.

3. The decreases of water vapor and aerosol at 410 K

As we see in Fig. 3, the simultaneous decreases of aerosol and water vapor at 410 K are found when the balloon travels through the vortex edge region. This is a favorable condition for our study and deserves some comments concerning what we consider as the vortex edge region.

The precise identification and localization of the vortex edge is not always straightforward and depends on the problem under study. Rummukainen et al. (1994) compared the use of the wind maximum and the use of the maximum isentropic Ertel Potential Vorticity (EPV) gradient for determination of the vortex edge. They found that both quantities give similar results. Other authors suggest the use of chemical definitions (Proffitt et al., 1989) or simply a fixed value of EPV on an isentropic surface.

McIntyre and Palmer (1983, 1984), Butchart

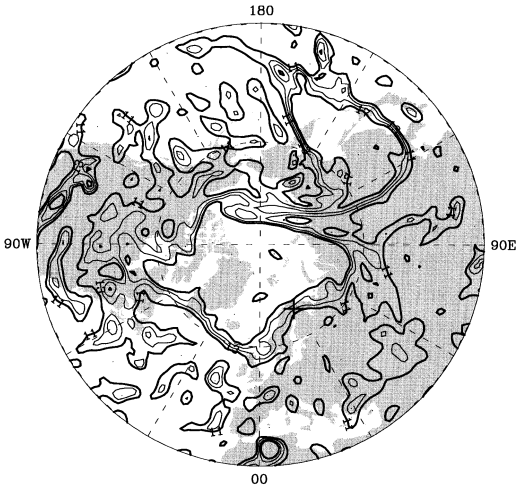

Fig. 3. Ertel potential vorticity at the 410 K level on 13 February 1995 at 18 UTC. The cross indicates the position of the measured air parcel. EPV contours are drawn at intervals of 2 EPV units (EPVU), on the vortex edge region. Thick isolines correspond to its equatorward and poleward boundaries.

and Remsberg (1986), Trounday et al. (1995) and Nash et al. (1996) have used other methods, based on the area variation of the stratospheric vortex. These methods consist in associating an EPV value to a surface element at each point of some grid. By summation of the surface elements, it is possible to compute the area as a function of EPV value. Going from high to low values of EPV, one finds a value at which the derivative of the area as a function of EPV increases abruptly. This defines the vortex area. The abrupt increase of the area derivative is due to the structure of the vortex, which consists in a high EPV gradient on isentropic surfaces surrounded by the "surf zone" where EPV isolines are less structured and sparser. In the surf zone, the EPV gradients are comparatively weaker due to the existence of planetary-wave breaking which destroys material contours (McIntyre and Palmer, 1984).

Teitelbaum et al. (1998) used 2 methods to define the outer boundary of the vortex edge: one is a slightly modified version of the area method of McIntyre and Palmer (1994), the other is a local method which we shall use here. This latter method consists in looking at the latitudinal variation of the absolute value of the EPV gradient (EPVG) at a given longitude. The EPVG is defined as:

$$\mathrm{EPVG} \equiv |\mathrm{grad}_\theta \mathrm{EPV}| \qquad (1)$$

and we define EPVG units $\equiv 10^{-11}$ m K $(\mathrm{kg\ s})^{-1}$.

We then search the 2 maxima of the EPVG slope, that is the maxima of the EPVG derivative along the selected meridian. Fig. 4 displays the results obtained for the EPVG and EPVG slope along the 28°E longitude meridian. This meridian corresponds to the longitude reached by the balloon during the descending part of its flight. We see that the air parcel is found between 2 maxima of the EPVG slope. The equatorward maximum is easily explained by the contrast between the vortex and the surf-zone. The poleward maximum is less evident because the EPVG variation is lower on this side. Commonly, other maxima of the EPVG slope appear, particularly in the surf zone, due to irregularities in the EPV. Nevertheless, it is easy to localize the boundaries of the edge region by comparing the results of Fig. 4 and the localization of the air parcel as seen in Fig. 3.

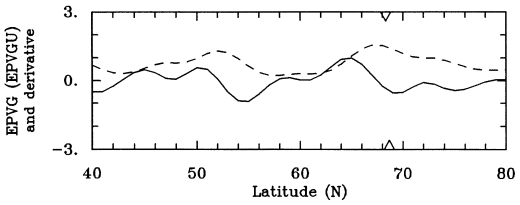

Fig. 4. Results of the calculation performed to determine the latitude of the outer and inner boundaries of the vortex edge region along the 28°E meridian. The dashed line represents EPVG and the full line its derivative. The arrows are at the latitude of the air parcel.

As has been shown in Teitelbaum et al. (1998), an air parcel can remain trapped inside the vortex edge for several days. In the present case, we shall show that in fact the air parcel studied was effectively trapped in the vortex edge for at least 7 days before its characteristics were measured on 13 February. This is a consequence of the quasi-impermeability of the vortex edge (McIntyre, 1989, 1995; Pyle, 1995). This also enables use to use backward trajectories to know the air parcel history with more confidence that in other cases.

The isentropic backward trajectories were computed with a dedicated numerical code developed in LMD. The code uses as input analyzed fields, given by the ECMWF, for temperature and velocities on 10 isobaric levels between 500 and 30 hPa. Data are given every 6 h on a regular 1.125° latitude–longitude grid. These values are then vertically interpolated to obtain velocity fields on an isentropic surface. Back trajectories are integrated using a 15-mn time step and a 2nd-order time marching technique. Interpolations in space and time were obtained using cubic splines. Fig. 5 displays some backward isentropic trajectories, computed with this code. All trajectories end on 13 February 1995 at or near the place of measurement, but always inside the vortex edge region.

Figs. 6, 7 display maps of EPV at 410 K for 9 and 6 February, respectively. On 9 February, the EPV isolines are very close to each other in the region where our air mass was traced back; this is evidently inside the vortex edge region as defined above. On 6 February, we can consider that the air mass was already in the vortex edge if we admit that the edge was then dilated between 80°E and 110°E longitudes. Such a type of dilation has been shown to occur, by Teitelbaum et al. (1998), as a consequence of the upwelling of the isentropic surface. This effect is demonstrated by defining

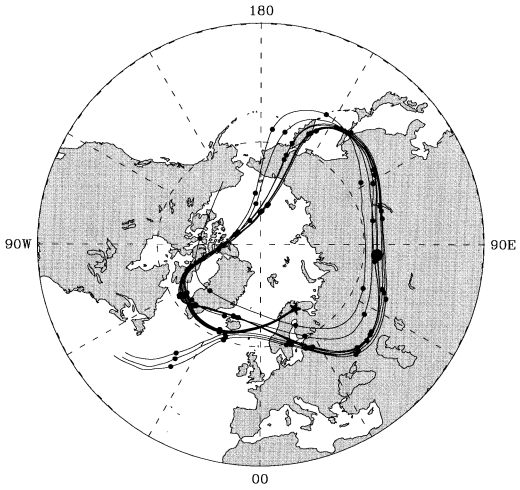

Fig. 5. Isentropic back trajectories computed at the 410 K level ending on 13 February 1995 at 18 UTC near the measurement point (68.5°N, 28°E). Small dots on the trajectories indicate daily positions; the larger dot indicates the location of the presumed PSC.

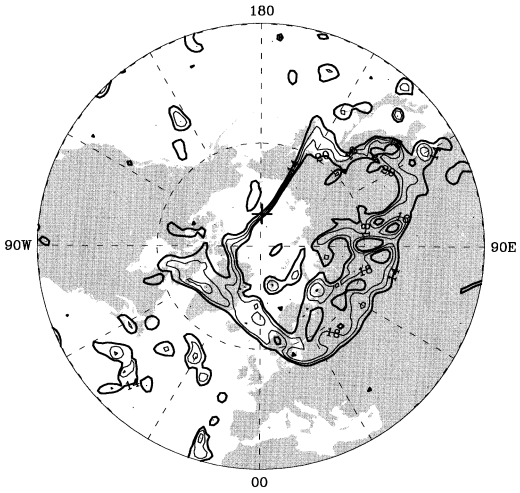

Fig. 6. The same as Fig. 3, but on 9 February 1995 at 18 UTC. The cross indicates the position of the air parcel given by the back trajectory shown in Fig. 5.

the isentropic density σ as:

$$\sigma = \rho \frac{\partial z}{\partial \theta} = -\frac{1}{g}\frac{\partial p}{\partial \theta}, \tag{2}$$

where ρ is density, p pressure, θ potential temperature, g the acceleration of gravity and σ the unit area on the isentropic surface in a layer of potential temperature thickness 1 K. The σ units are kg m^{-2} K^{-1}.

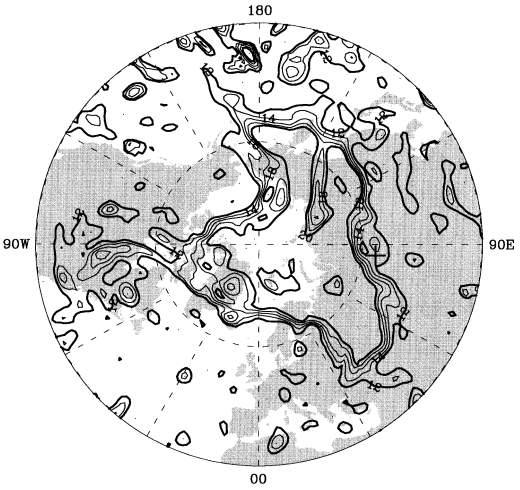

Fig. 7. The same as Fig. 3, but on 6 February 1995 at 18 UTC. The cross indicates the position of the air parcel given by the back trajectory shown in Fig. 5.

Consider a small material surface of area δs lying on an isentrope. In an adiabatic motion, this small surface moves with the fluid but remains on the same isentrope. Its area changes according to

$$\frac{\mathrm{D}}{\mathrm{D}t}\delta s = \nabla_\theta \cdot \boldsymbol{u}\, \delta s, \tag{3}$$

where $\mathrm{D}/\mathrm{D}t$ is the material derivative on the isentropic surface and $\boldsymbol{u}$ the velocity vector. The continuity equation for σ is:

$$\frac{1}{\sigma}\frac{\mathrm{D}\sigma}{\mathrm{D}t} + \nabla_\theta \cdot \boldsymbol{u} = 0. \tag{4}$$

Combining (3) and (4), we obtain:

$$\frac{\mathrm{D}}{\mathrm{D}t}\delta s = -\frac{1}{\sigma}\frac{\mathrm{D}\sigma}{\mathrm{D}t}\delta s. \tag{5}$$

Expression (5) shows that when a small surface lying on an isentrope goes upward (downward), as a consequence of an adiabatic deformation of the isentrope, the surface area increases (decreases) and EPV isolines separate.

Fig. 8 shows that in our case, on 6 February, the geopotential on the 410 K surface is the highest in vicinity of the position of the air parcel. Moreover, as shown in Teitelbaum and Sadourny (1998), the upwelling of the isentropic surface and

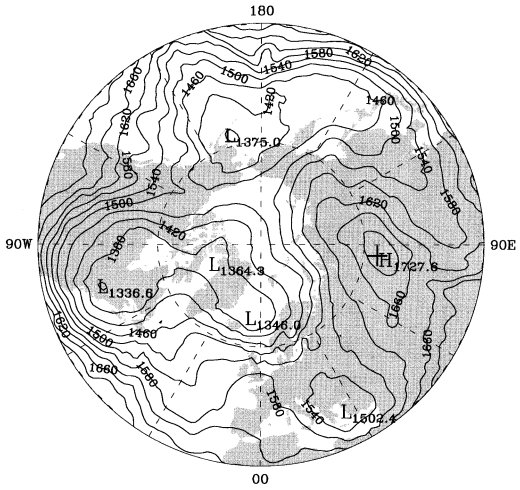

Fig. 8. Geopotential isolines calculated from ECMWF analysis at the 410 K level on 6 February 1995. The cross indicates the position of the air parcel given by the back trajectory shown in Fig. 5. The contour interval is 40 dam.

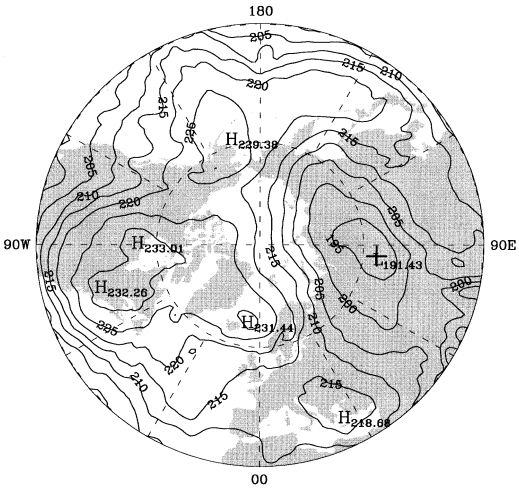

Fig. 9. Temperature isolines calculated from ECMWF analysis at the 410 K level, 6 February 1995. The cross indicates the position of the air parcel given by the back trajectory shown in Fig. 5. The contour interval is 5 K.

the associated decrease of temperature favor the formation of PSCs. Indeed, taking into account the adiabatic relation:

$$c_p \, \Delta T = -g \, \Delta z, \tag{6}$$

which links the cooling to the upwelling of the isentropic surface; the temperature of the air mass must be minimum there, and this is the case as can be seen in Fig. 9. Now, we will show that the cooling there was sufficient for PSC formation.

The main types of PSCs are first those formed by 3 water molecules associated with one molecule of nitric acid, namely nitric acid trihydrate (NAT or type I), and second that comprising water or ice PSCs (type II). A decrease of more than 10% in water vapor cannot be due to a NAT formation. As the water vapor is more abundant than nitric acid by a factor of approximately 500, the water vapor pressure would remain relatively unperturbed, while the nitric acid pressure can be deeply lowered, as the trihydrate condenses (Hanson and Mauersberger, 1988). The simultaneous decrease of water vapor and aerosol can only be due to an ice PSC formation, which on the other hand, has a formation time shorter than NAT. A strong water vapor loss in the Arctic vortex has been shown by Vömel et al. (1977), to be a consequence of an ice PSC formation.

At the place and time of our measurement, the conditions are far from that usually admitted for ice PSC formation; the measured temperature is 198 K, a value which is too high to allow the formation of an ice PSC (Marti and Mauersberger, 1993; Emanuel, 1994). Conversely, on 6 February, as deduced from the ECMWF analysis, the air mass was submitted to a temperature decrease, reaching a value close to the temperature required for PSC type II formation. Moreover, it must be taken into account that, as stated by Knudsen et al. (1996), during the 1994–1995 winter, the potential for PSC formation, including ice PSCs, was in reality much larger than that predicted from ECMWF temperatures. The temperature differences, found by comparison of ECMWF analysis and long-duration balloon data or radiosondings, are of 2.4 K in the mean, but can be up to 6 K at local minima.

Fig. 10 shows the temperature profile obtained from ECMWF analysis on 6 February at 18 UTC at the air parcel position. We can see that the minimum temperature in the profile is found at the level 410 K, with a value very close to the PSC II temperature formation. The possible mean temperature deviations, from the results of Knudsen et al. (1996), are also plotted. The Knudsen (1996) conclusions concerning the low Arctic temperature found during the winter

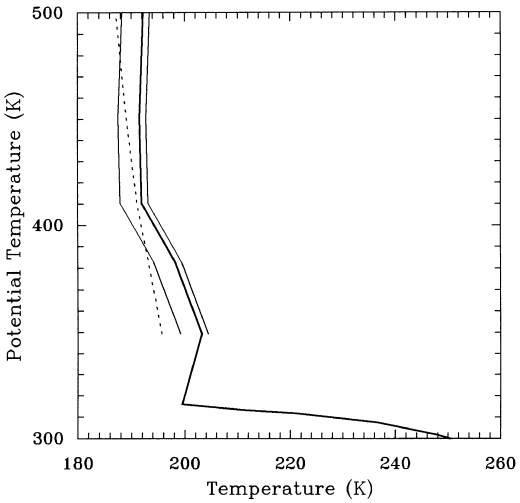

Fig. 10. Temperature profile as a function of potential temperature from the ECMWF analysis at the position of the air parcel on 6 February 1995 (thick full line) The thin full lines indicate other possible temperature profiles taking into account the bias found by Knudsen et al. (1996). The dotted line is the temperature threshold for ice PSC formation.

1994/1995 agree with the study carried out by Naujokat and Pawson (1996) and Pawson and Naujokat (1999). These authors showed that low stratosphere temperatures in the northern winters 1994/1995, 1995/1996 and 1996/1997 were low enough to support PSC formation for prolonged periods. Moreover they claimed that occasionally the temperature reached values low enough for ice-cloud formation. Pawson et al. (1999), looking for the regions of lowest temperature in the Arctic during the period 1981–1996, found that the region where the temperature reached values lower than the ice PSC formation in February, lies over Siberia. Note that the site where we suggest the PSC formation was over Siberia.

These results strongly suggest that the temperature on 6 February at the 410 K level was actually lower than that given by ECMWF in Fig. 10, and low enough for the formation of an ice PSC.

Furthermore, the TOVS total ozone analysis on 6 February (Fig. 11) displays a decrease of ozone at the very place we presume a PSC exists. PSCs and local decrease of ozone are known to be found simultaneously, and it has been shown by Teitelbaum and Sadourny (1998), that this simultaneity is mainly due to the upwelling of isentropic surfaces. This further supports our hypothesis of the occurrence of a PSC at this time and place.

Once the PSC is formed, the air parcel must spend a sufficient time in these conditions for significant dehydration and sedimentation. The PSC ice particles have diameters between 10 to 100 μm and the smallest one can fall 2 km per day (Turco et al., 1989). They carry, while falling, the aerosol which served as condensation nucleus for their formation (Toon et al., 1989). Temperature profiles from the ECMWF (not shown here) indicate that conditions similar to those in Fig. 10, occurred at least up to 6 h before and 3 h after, that is to say at least for 9 h. We don't know the actual particle size to perform a precise calculation of the sedimentation distance, but we think that this time must be sufficient to explain the small decrease in aerosol and water vapor.

One can ask about the fate of the water after sedimentation. We do not expect to see it in lower layers in the measured profile, because the vertical wind shears might spread the sedimented water over an extended region.

All these results suggest that the air mass encountered at 410 K on 13 February was processed by a PSC on 6 February, and this explains the decrease of water vapor and aerosol measured at this level.

4. The decreases of water vapor and aerosol at 364 K

We searched without success a local cause to explain the water vapor and aerosol decreases at the 364 K level. We then studied the possibility that the considered air parcel originates from far off the site of measurement. This air parcel is, when measured, at the sub-vortex level, where air masses are mainly transported by Rossby waves. The back trajectory displayed in Fig. 12 shows that the air mass can have its origin, 9 days before, at middle latitudes (around 37°N). Such a back trajectory is indeed more subject to caution than that of the 410 K level; however, confidence in it can be enhanced by a careful inspection of some properties of the air mass along the trajectory. During this time, between 4 and 13 February, the air mass remains constantly in the lowermost stratosphere, as defined by Holton et al. (1995). The measured water vapor mixing ratio is very

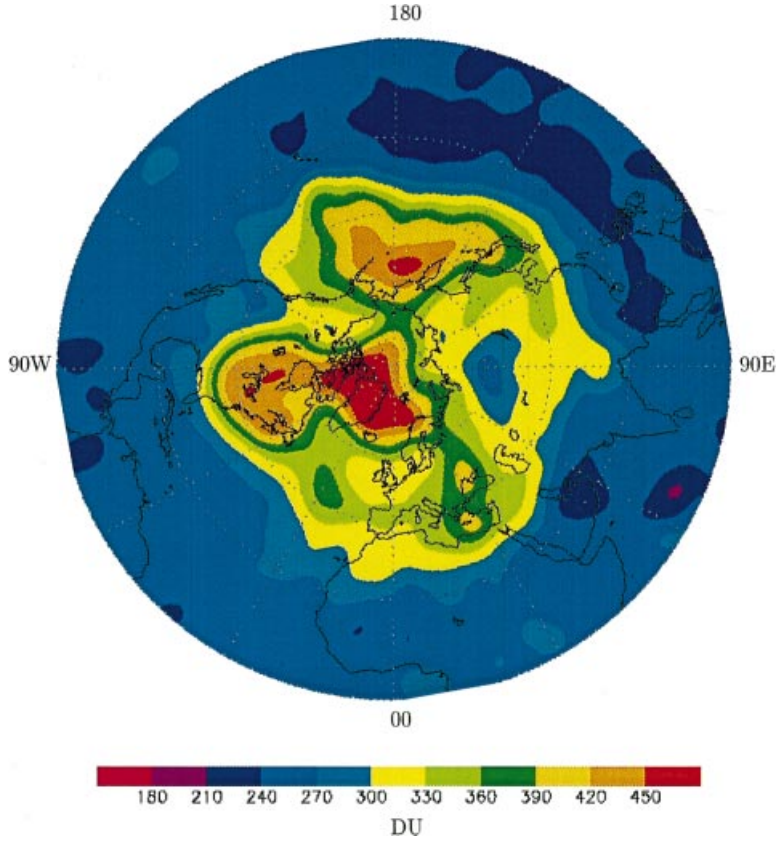

Fig. 11. TOVS total ozone analysis (in Dobson units) as retrieved by the Climate Analysis Center on 6 February 1995.

low even for 37°N. This value is not far from those found at the hygropause, typical of tropical latitudes, where they are consequences of deep convective phenomena (Kley et al., 1982). However, it is known that in the range 22 to 28 km, the horizontal mixing between the tropics and the extra tropics is highly inhibited by a transport barrier (Trepte and Hitchman, 1992; Chen et al., 1994). Nevertheless, as shown by Kar and Mahajan (1998), some water vapor profiles obtained at mid-latitudes from the Stratospheric Aerosol and Gas Experiment (SAGE II), present maxima and minima similar to those found in the tropics, and were called "tape recorder" by Mote et al. (1996). Those structures, following Kar and Mahajan (1998), are a consequence of occasional transport of air from the tropics to mid-latitude in the form of tongues. Here, we are interested in the lower stratospheric level of this structure as, after the back trajectory, the air mass with low water vapor content at 364 K should come from mid-latitudes. Further, it is worthwhile noting that in the data obtained by Kar and Marhajan (1998), values of 2.5 to 3 ppmv of water vapor mixing ratio were found at 15 to 17 km altitude, that is at the approximate altitude of the air parcel on 4 February 1995 at the 364 K level.

Thus, we will make the hypothesis that the air parcel found on 13 February at the 364 K level was on 4 February at 37°N latitude. To further test the validity of this hypothesis, we shall compare some characteristics measured in the air mass to those it had on 4 February at the place indicated by the 364 K back trajectory. In Fig. 1, we can see that in the layer between both laminae, for instance at the 389 K level, there is no decrease of water vapor or aerosol. We shall then search for the origin of the air mass at this intermediate level

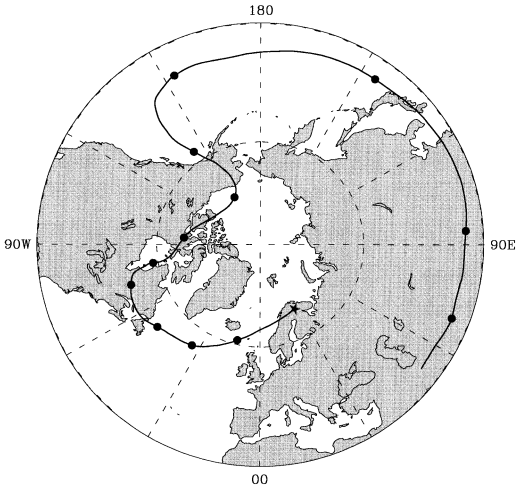

Fig. 12. Isentropic back trajectory computed at the 364 K level ending on 13 February 1995 at 18 UTC at the measurement point (68°N, 28°E). Dots on the trajectories indicate daily positions.

and compare the result to that of the 364 K level. The isentropic back trajectory for the 389 K level air mass is displayed in Fig. 13. Let us look at the characteristics, on 5 February, of this 389 K air mass. This date has been chosen, because the air mass was then at its lowest latitude and should have its lowest water vapor value. Fig. 14 displays 3 EPV profiles obtained from the ECMWF analysis. The solid line corresponds to the measurement point (13 February), the dashed line to the 389 K back trajectory position on 5 February, and the dotted line to the 364 K back trajectory position on 4 February. We can see that, at the 364 K level, the EPV value at the measurement point and date is very close to that on 4 February at the 364 K back trajectory end-point. A similar result is obtained by comparing the values for the 389 K level, at the measurement point and at the 389 K back trajectory end-point on 5 February. EPV profiles have been used by Vaughan and Timmis (1998) to show that air masses with very low ozone mixing ratio have a tropospheric origin. In the case under study, we can see, taking into account the EPV values, that the origin of the air mass is stratospheric.

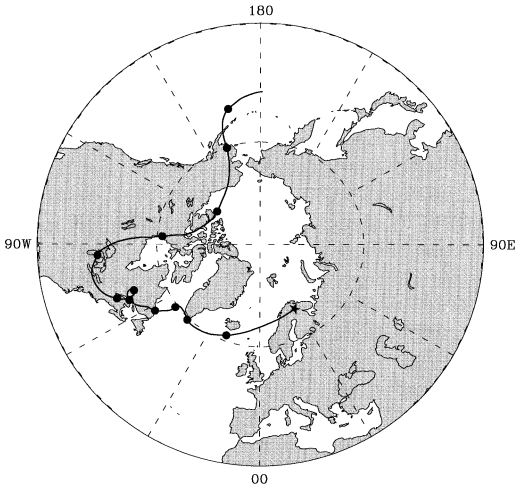

Fig. 13. Same as Fig. 12, but at the 389 K level.

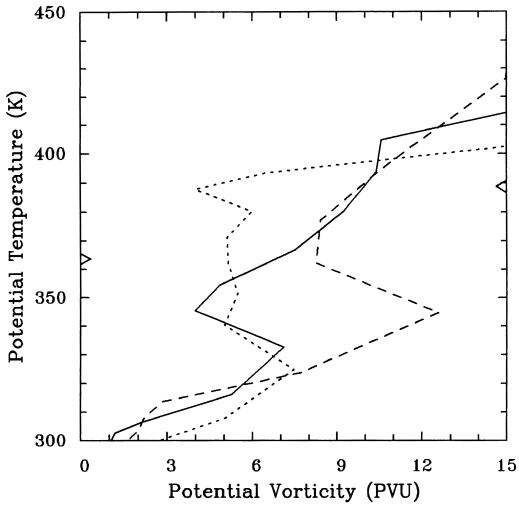

Fig. 14. EPV profiles calculated from ECMWF analysis: on 13 February 1995 at 68°N, 28°E (full line, measurement point and date), on 5 February at 44°N, 274°E (dashed line, 389 K back trajectory end-point) and on 4 February at 37°N, 209°E (dotted line, 364 K back trajectory end-point).

In fact, the tropopause is defined by the World Meteorological Organization (WMO) as the lower boundary of the lowest layer in which the temperature lapse rate is less than 2°C/km for a depth of at least 2 km. It has been suggested by Danielsen (1968) that with this conventional definition, the tropopause location can have large and erratic variations because adiabatic motions do not conserve the stability. He shows that the potential vorticity (PV), because of its conservative

characteristics, is more convenient for the determination of the location of the tropopause, and proposed a value between 2 and 3 potential vorticity units ($1\ \mathrm{PVU} = 10^{-6}\ \mathrm{K\ m^2\ kg^{-1}\ s^{-1}}$). Later Hoskins (1991) used 2 PVU to locate the tropopause and Hoerling et al. (1991), following a study based on analyzed ECMWF data, conclude that 3.5 PVU represents an optimal value for the tropopause level outside the tropics. In the case studied here, the Hoerling et al. (1991) definition shows the stratospheric origin of the air mass studied.

To compare water vapor mixing ratios, we used the HALOE data from the Upper Atmospheric Research Satellite (UARS). For 5 February the data can be found in the HALOE records. Unfortunately, this is not the case for 4 February at the site indicated by the 364 K back trajectory. We used instead the mean of the 2 nearest in time and place data. The result of the comparison is displayed in Fig. 15. As for the EPV, the water vapor mixing ratios are nearly conserved at both levels, and this confirms that the air mass whose characteristics where measured on 13 February at 364 K, comes from middle latitudes.

The decrease in aerosol can also be explained by the origin of the air mass. In fact, HALOE data show that during February 1995, the extinction coefficient near 364 K was lower at middle than at higher latitudes.

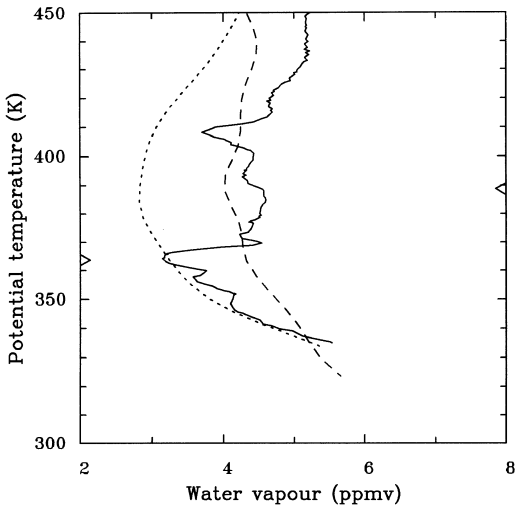

Fig. 15. Water vapor profiles from measurements on 13 February 1995 (full line, measurement point and date), from HALOE data on 5 February at 44°N, 274°E (dashed line, 389 K back trajectory end-point) and from a mean of values close to 37°N, 209°E, 4 February (dotted line, 364 K back trajectory end-point).

It can be argued that diabatic phenomena such as breaking of Rossby waves (McIntyre and Palmer, 1984) should mix the air masses during their transport. We think that some partial mixing must occur, but without completely destroying the individuality of air masses: they preserve many of their characteristics. To support this hypothesis, we shall show the Montgomery potential at the 364 K level on 4 and 13 February 1995. The Montgomery potential is defined by:

$$M = c_p T + \phi, \tag{7}$$

where c_p is the heat capacity at constant pressure, T temperature and ϕ geopotential. On an isentropic surface, the Montgomery potential is the streamfunction of the geostrophic wind, which then blows along its isolines. Figs. 16a,b display the Montgomery potential at the 364 K level for 4 and 13 February, respectively. Crosses have been drawn at the geographical locations of the studied air mass. Comparing the isolines with the starting and ending points of the trajectory, we can see that our air mass was transported mainly by the geostrophic wind. The geostrophic wind is induced by long-period Rossby waves. It is clear in both figures that the main wave is a long period, no. 3, wave.

All these results (similarity of EPV and water vapor at both places on 4 and 13 February, aerosol variation with latitude and air masses driven by a wind very close to the geostrophic one), support our hypothesis on the origin of the air mass found at the 364 K level on 13 February, and explain the laminae encountered in the measurement.

5. Conclusion

Two simultaneous water vapor and aerosol laminae were found during a measurement performed by an instrumented balloon launched from Kiruna. Despite the similarity of both phenomena, we showed that their causes are different. One of the laminae was encountered when the balloon traveled through the vortex edge region as defined locally. We showed that this air mass has been trapped for several days in the vortex edge, and has been processed by a PSC that caused the

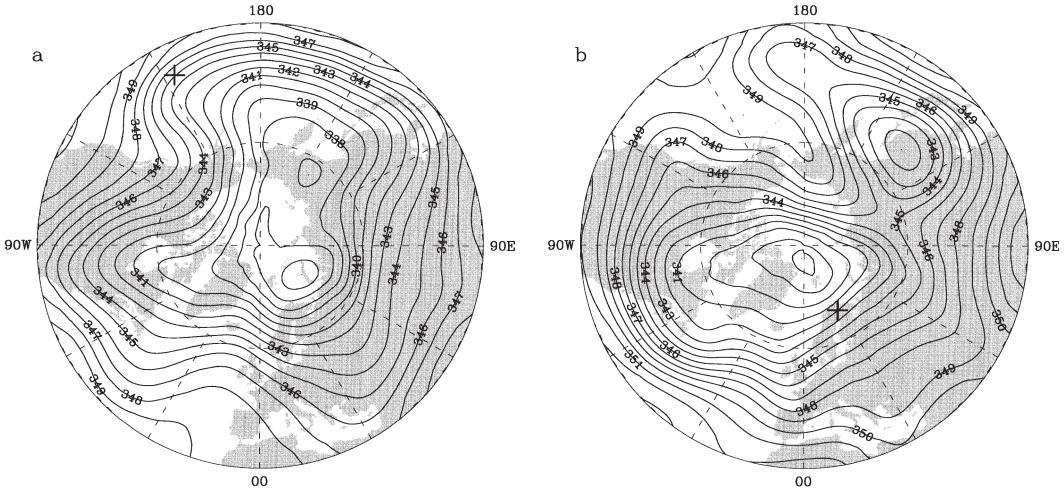

Fig. 16. Montgomery potential at the 364 K level on 4 February (a) and on 13 February (b). Crosses indicate the locations of the air parcel. The contour interval is 10^3 m^2 s^{-2}.

decrease of water vapor and aerosol. The other laminae were found in the sub-vortex region. As research of local causes has been unsuccessful, we searched for a possible origin of the air parcel. Although the back trajectories in these conditions are more subject to caution, comparison of several characteristics of the air mass, such as potential vorticity, water vapor mixing ratio and aerosol content, support the hypothesis that this air parcel came from middle latitudes and had the signature of this region. Furthermore, observations of the Montgomery potential show that this air parcel had been transported by a wind very close to the geostrophic wind, which guarantees the conservation of the parcel individuality.

The present study has then explained for the first time, laminae encountered simultaneously in water vapor and aerosol; further, it showed that the causes of the laminae can be very different, one being due to a local PSC interaction, the other due to transport from middle latitudes.

6. Acknowledgments

We acknowledge the European Center for Medium-range Weather Forecasts (ECMWF), which provided the data analysis, and the HALOE science team for water vapor and aerosol data. The TOVS total ozone maps were provided by the NOAA Climate Analyses Center. We acknowledge J. Ovarlez from the LMD technical group for water vapor and aerosol soundings.

REFERENCES

Brasseur, G. and Solomon, S. 1998. *Aeronomy of the middle atmosphere*. D. Reidel Publishing Company, 436 pp.

Butchart, N. and Remsberg, E. E. 1986. The area of the stratospheric polar vortex as a diagnostic for tracer transport on an isentropic surface. *J. Atmos. Sci.* **43**, 1319–1339.

Chen, P., Holton, J. R., O'Neill, A. and Swinbank, R. 1994. Quasi-horizontal transport and mixing in the Antarctic stratosphere. *J. Geophys. Res.* **99**, 16,851–16,866.

Danielsen, E. F. 1968. Stratospheric–tropospheric exchange based in radioactivity, ozone and potential vorticity. *J. Atmos. Sci.* **25**, 502–518.

Dobson, G. 1973. The laminated structure of the ozone in the atmosphere. *Q. J. R. Meteorol. Soc.* **99**, 599–607.

Emanuel, K. A. 1994. *Atmospheric convection*. Oxford University Press, 580 pp.

Hanson, D. R. and Mauersberger, K. 1988. Laboratory studies of the nitric acid trihydrate: implication for the South Polar Stratosphere. *Geophys. Res. Lett.* **15**, 855–858.

Hoêrling, M. P., Schaack, T. K. and Lenzen, A. J. 1991. Global objective tropopause analysis. *Mon. Wea. Rev.* **119**, 1816–1831.

Holton, J. R., Haynes, P. H., McIntyre, M. E., Douglass, A. R., Rood, R. and Pfister, L. 1995. Stratosphere–troposphere exchange. *Rev. of Geophys.* **33**, 403–439.

Hoskins, B. J. 1991. Towards a PV-θ view of the general circulation. *Tellus* **43A/B**, 27–35.

Jost, H., Lowenstein, M., Pfister, L., Margitan, J. J., Chang, A. Y., Salawitch, R. J. and Michelsen, H. A. 1998. Laminae in the tropical middle stratosphere: origin and age estimation. *Geophys. Res. Lett.* **25**, 4337–4340.

Kar, J. and Mahajan, K. K. 1998. Evidence of transport in water vapor profiles at mid-latitudes from Stratospheric Aerosol and Gas Experiment (SAGE II) measurements. *J. Geophys. Res.* **103**, 31,057–31,065.

Kley, D., Drummond, J. W. and Schmeltekopf, A. L. 1980. On the structure and microstructure of stratospheric water vapor. In: *Atmospheric water vapor* (eds. Deepak, A., Wilkerson, T. D. and Runke, L. H.). Academic Press (New York), p. 315.

Kley, D., Schmeltekopf, A. L., Kelly, K., Winkler, R. H., Thomson, T. L. and McFarland, L. 1982. Transport of water vapor through the tropical tropopause. *Geophys. Res. Lett.* **9**, 617–620.

Knudsen, B. M., Rosen, J. M., Kjome, N. T. and Whitten, A. T. 1996. Comparison of analyzed stratospheric temperatures and calculated trajectories with long-duration balloon data. *J. Geophys. Res.* **101**, 19,137–19,145.

Knudsen, B. M. 1996. Accuracy of arctic stratospheric temperature analyses and the implication for the prediction of polar stratospheric clouds. *Geophys. Res. Lett.* **23**, 3747–3750.

Manney, G. L., Bird, J. C., Donovan, D. P., Duck, T. J., Whiteway, J. A., Pal, S. R. and Carswell, A. I. 1998. Modeling ozone laminae in ground-based Arctic wintertime observations using trajectory calculations and satellite data. *J. Geophys. Res.* **103**, 5797–5814.

Mariotti, A., Moustaoui, M., Legras, B. and Teitelbaum, H. 1997. Comparison between vertical ozone soundings and reconstructed potential vorticity maps by contour advection and surgery. *J. Geophys. Res.* **102**, 6131–6142.

Marti, J. and Mauersberger, K. 1993. Laboratory simulations of PSC particule formation. *Geophys. Res. Lett.* **20**, 359–362.

Mastenbrook, H. J. 1968. Water vapor distribution in the stratosphere and high troposphere. *J. Atmos. Sci.* **25**, 299–311.

McIntyre, M. E. and Palmer, T. N. 1983. Breaking planetary waves in the stratosphere. *Nature* **305**, 593–600.

McIntyre, M. E. and Palmer, T. N. 1984. The "surf zone" in the stratosphere. *J. Atmos. Terr. Phys.* **46**, 825–849.

McIntyre, M. E. 1989. On the Antarctic ozone hole. *J. Atmos. Terr. Phys.* **51**, 29–43.

McIntyre, M. E. 1995. The stratospheric polar vortex and sub-vortex: fluid dynamics and mid-latitude ozone loss. *Phil. Trans. R. Soc. London* **A352**, 227–240.

Mote, P. W., Rosenlof, K. H., McIntyre, M. E., Carr, E. S., Gille, J. C., Holton, J. R., Kinnersley, J. S., Pumphrey, H. C., Russel III, J. M. and Waters, J. W. 1996. The imprint of tropical tropopause temperatures on stratospheric water vapor. *J. Geophys. Res.* **101**, 3989–4006.

Nash, E. R., Newman, P. A., Rosenfeld, J. E. and Schoeberl, M. R. 1996. An objective determination of the polar vortex using Ertel's potential vorticity. *J. Geophys. Res.* **101**, 9471–9478.

Naujokat, B. and Pawson, S. 1996. The cold stratospheric winters 1994/1995 and 1995/1996. *Geophys. Res. Lett.* **23**, 3703–3706.

Newman, P. A., Lait, L. R., Scoeberl, M. R., Seablom, M., Coy, L., Rood, R., Swinbank, R., Proffitt, M., Loewenstien, M., Podolske, J. R., Elkins, J. W., Webster, C. R., May, R. D., Fahey, D. W., Dutton, G. S. and Chan, K. R. 1996. *J. Geophys. Res.* **101**, 12,879–12,891.

Orsolini, Y. J., Hansen, G., Hoppe, U. P., Manney, G. L. and Fricke, K. H. 1997. *J. Geophys. Res.* **123**, 785–800.

Orsolini, Y. J., Manney, G. I., Engel, A., Ovarlez, J., Claud, C. and Coy, L. 1998. Layering in stratospheric profiles of long-lived trace species: balloon-borne observations and modelling. *J. Geophys. Res.* **103**, 5815–5825.

Ovarlez, J., Brioit, B., Capus J. and Ovarlez, H. 1987. Developpement et essais en vol ballon d'un hygrometre a point de rosée pour sondage de l'atmosphère. *Bull. Bur. Natl. Metrologie* **69**, 9–14.

Pawson, S. and Krüger, K., Swinbank, R., Balley, M. and O'Neill, A. 1999. Intercomparison of two stratospheric analyses: temperatures relevant to polar stratospheric cloud formation. *J. Geophys. Res.* **104**, 2041–2050.

Pawson, S. and Naujokat, B. 1999. The cold winters of the middle 1990s in the northern lower stratosphere. *J. Geophys. Res.* **104**, 14,209–14,222.

Proffitt, M. H., Powell, J. A., Tuck, A. F., Fahey, D. W., Kelly, K. K., Krueger, A. J., Schoeberl, M. R., Gary, B. L., Margitan, J. J., Chan, K. R., Loewenstein, M. and Podolske, J. R. 1989. A chemical definition of the boundary of the Antarctic ozone hole. *J. Geophys. Res.* **94**, 11,437–11,448.

Pyle, J. A. 1995. Ozone loss in middle latitudes and the role of the Arctic polar vortex. *Phil. Trans. R. Soc. London* **A352**, 241–245.

Reid, S., Vaughan, G. and Kyro, E. 1993. Occurrence of ozone laminae near the boundary of the stratospheric polar vortex. *J. Geophys. Res.* **98**, 8883–8890.

Rummukainen, M., Knudsen, B. and Von der Gathen, P. 1994. Dynamical diagnostics of the edges of the polar vortices. *Ann. Geophys.* **12**, 1114–1118.

Teitelbaum, H., Moustaoui, M., Ovarlez, J. and Kelder, H. 1996. The role of atmospheric waves in the laminated structure of ozone profiles at high latitudes. *Tellus* **48A**, 442–455.

Teitelbaum, H. and Sadourny, R. 1998. The role of planetary waves in the formation of polar stratospheric clouds. *Tellus* **50A**, 302–312.

Teitelbaum, H., Moustaoui, M., Van Velthoven, P. F. J. and Kelder, H. 1988. Decrease of total ozone at low latitudes in the southern hemisphere by a combination of linear and nonlinear processes. *Q. J. R. Meteorol. Soc.* **124**, 2625–2644.

Toon, O. B., Turco, R. P., Jordan, J., Goodman, J. and Ferry, G. V. 1989. Physical processes in polar stratospheric clouds. *J. Geophys. Res.* **94**, 11,359–11,380.

Trepte, C. R. and Hitchman, M. H. 1992. Tropical stratospheric circulation deduced from satellite aerosol data. *Nature* **355**, 636–628.

Trounday, B., Perthuis, L., Strebelle, S., Farrara, J. D. and Mechoso, C. R. 1995. Dispersion properties of the flow in the southern stratosphere during winter and spring. *J. Geophys. Res.* **100**, 13,901–13,917.

Turco, R. P., Toon, O. B. and Hamil, P. 1989. Heterogeneous physico-chemistry of the polar ozone hole. *J. Geophys. Res.* **94**, 16,493–16,510.

Vaughan, G. and Timmis, C. 1998. Transport of near-tropopause air into the lower midlatitude stratosphere. *Q. J. R. Meteorol. Soc.* **124**, 1559–1578.

Vömel, H., Rummukainen, M., Kivi, R., Karhu, J., Turunen, T., Kyro, E., Rosen, J., Kjome, N. and Oltmans, S. 1997. Dehydration and sedimentation of ice particles in the Arctic stratospheric vortex. *Geophys. Res. Lett.* **24**, 795–798.